CFD ANALYSIS OF EMISSIONS FOR A CANDIDATE N+3 COMBUSTOR

Kumud Ajmani
Vantage Partners, LLC
Cleveland, Ohio, USA

ABSTRACT

An effort was undertaken to analyze the performance of a model Lean-Direct Injection (LDI) combustor designed to meet emissions and performance goals for NASA's N+3 program. Computational predictions of Emissions Index (EINOx) and combustor exit temperature were obtained for operation at typical power conditions expected of a small-core, high pressure-ratio (>50), high T_3 inlet temperature (>950K) N+3 combustor. Reacting-flow computations were performed with the National Combustion Code (NCC) for a model N+3 LDI combustor, which consisted of a nine-element LDI flame-tube derived from a previous generation (N+2) thirteen-element LDI design. A consistent approach to mesh-optimization, spray-modeling and kinetics-modeling was used, in order to leverage the lessons learned from previous N+2 flame-tube analysis with the NCC. The NCC predictions for the current, non-optimized N+3 combustor operating indicated a 74% increase in NOx emissions as compared to that of the emissions-optimized, parent N+2 LDI combustor.

1.0 INTRODUCTION

NASA's Environmentally Responsible Aviation (ERA) program [Lee 2007] has revived interest in Lean-Direct Injection (LDI) combustor concepts due to the low emissions achieved with these injectors in previous development efforts [Tacina 2005]. LDI combustors are characterized by all of the *combustion* airflow being introduced at the dome, followed by rapid fuel-air mixing and burning behind multiple injectors in a small area. Some highlights of current generation (LDI-2) experimental and CFD efforts have been reported by [Lee 2013], [Tacina 2014], [Zink 2014] and [Ajmani 2014a]. The success of LDI-1 and LDI-2 efforts undertaken to meet NASA's N+1 and N+2 emissions reductions targets, show that LDI technology is a worthy candidate to be potentially used in the design of small-core, high-pressure ratio combustors that can meet NASA's N+3 emissions goals.

Ideally, any current or future approach to a third-generation combustor design to meet NASA's N+3 emissions and performance goals will leverage the lessons learned from 1st and 2nd generation (LDI-1 and LDI-2) technology design efforts. CFD evaluation of injector elements consisting of a combination of axially (or radially) staged swirl-venturi and pressure atomizing or air-blast injectors will be used to optimize the LDI-3 injector element design. The individual injector elements will be modeled to be assembled into an array, which will then be fitted into a nominally 30% smaller core-size for an N+3 combustor as compared to an N+2 combustor. A combination of simplex and airblast injector elements arranged with varying radial and axial spacing, packing factor and combustor expansion ratio would be studied to optimize the performance and emissions goals of a candidate LDI-3 design.

In the current work, the National Combustion Code (NCC) was used to perform CFD simulations of a model N+3 combustor, derived from the design of a Woodward FST, Inc. N+2 combustor which was experimentally studied under the ERA program [Tacina 2014]. This paper describes some of the efforts undertaken with the NCC to build upon the *affordable* CFD best practices identified in [Ajmani 2013a], and apply said best practices to predict emissions (NOx, CO and unburnt hydrocarbons) for a model N+3 combustor. The primary motivation for using the NCC for N+3 CFD analysis is to leverage the technology lessons learned in N+2 design and analysis [Ajmani 2014a]. The long-term goal is to use NCC-driven CFD results to positively impact the design of flame-tube and arc-sector rig experiments, as also the eventual design of N+3 combustors that use LDI-1 and LDI-2 technology.

2.0 N+3 CONFIGURATION AND RESULTS

The model N+3 flame-tube design with nine injector-elements is shown in Figure 1. Each injector element consists of an air-swirler section with six passages formed by axially swirled blades followed by a venturi section. Fuel is injected at (or near) the throat of the venturi with a pressure-swirl atomizing (simplex) nozzle or a fuel-filming airblast nozzle. Note that the airblast elements contain an additional circuit of "inner" air-swirler (IAS) passages comprising of four axially swirled blades, located axially upstream of the six-blade primary "outer" air swirler passages (OAS). The expansion ratio and exit area for the central element (Pilot, P) (see figure 2) is larger than the surrounding eight elements, in order to provide better interaction with the other two stages (M1, M2), when operating in reduced power flight regimes where all the injection elements are not being fueled.

The model nine-element N+3 geometry studied here was derived by eliminating the four injector elements located at the corners of the thirteen-element 'flat-dome' configuration tested by Woodward FST, Inc. and NASA for the N+2 program

[Tacina 2014]. In order to meet the N+3 program's "smaller core-size" requirement, the core-size of the model N+3 combustor was reduced by 30% as compared to the N+2 combustor core. This area reduction was achieved by replacing the square cross-section dome (20.25 in^2, 4.5" x 4.5") of the N+2 design with a cylindrical flame-tube (D = 3.0"). This decrease in 30% combustor area, accompanied by the 30% reduction in effective area, ensured that the expansion ratio for the N+3 design was very similar to that for the N+2 design. Note that the model N+3 design lends itself to further reductions in core size if the spacing between the injectors at the dome were to be reduced. The effect of inter-injector spacing on combustor performance will be evaluated as a design parameter in future CFD analysis with the NCC code.

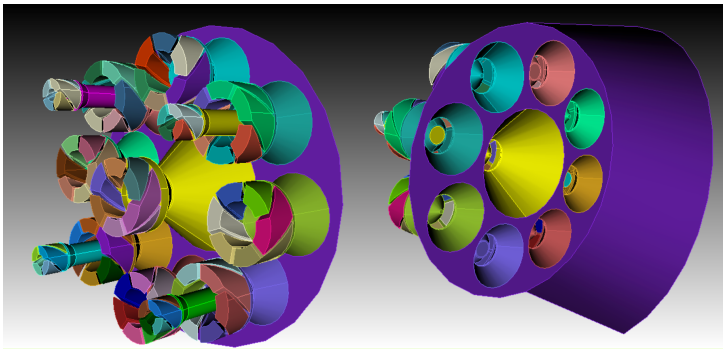

Figure 1. Geometry for a model 9-element N+3 configuration as derived from a 13-element N+2 configuration [Tacina 2014]

Some details of the model N+3 geometry and mesh are shown in figure 2. The Pilot (P) and two 'Main' (M1, M2) fuel-stages have their venturi-exit plane in-line with combustor dump-plane. These injection elements consist of:

- Pilot (P) stage: Simplex (pressure atomizer) tip, 55° CCW axially-bladed swirlers
- Main1 (M1) stage: 4 elements, Simplex fuel tips, 45° CCW axially-bladed swirlers
- Main2 (M2) stage: 4 elements, Airblast fuel tips, OAS/IAS 45° CW/45 ° CW

OAS/IAS refer to Outer/Inner Axial Swirl venturis, CW refers to Clockwise orientation, and CCW refers to Counter Clockwise orientation. In summary, the Pilot and Main1 stages fueled with simplex nozzles have co-rotating, axially bladed air swirlers (CCW direction). The Main2 stage fueled with airblast nozzles has two sets of outer and inner air passages with co-rotating (CW direction) axially bladed swirlers. Note that the air-swirlers in the Pilot and Main (M1) stages (CCW) are counter-rotating with respect to the air-swirlers in the Main2 (M2) stage (CW).

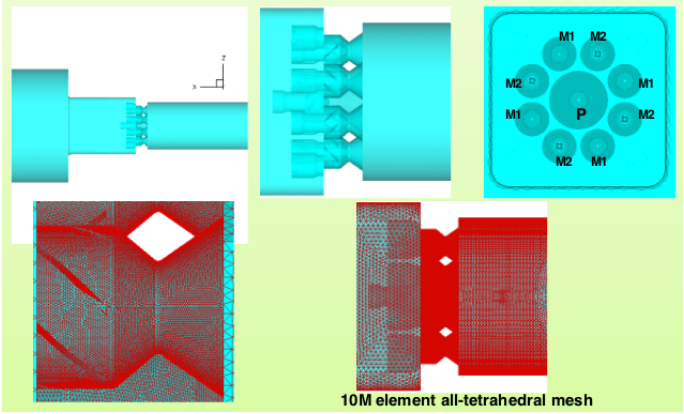

Figure 2. Geometry and mesh for a model N+3 configuration; M1, M2 are the two "Main" stages, P is the "Pilot"

3.0 COMPUTATIONAL TOOLS AND METHODS

The National Combustion Code (NCC) is a state-of-the-art computational tool that is capable of solving the three-dimensional, time-dependent, Navier-Stokes equations with an Eulerian, finite-volume formulation. For gas-turbine combustors, the injection of liquid-fuel droplets is modeled with a Lagrangian formulation. The combustion of fuel is modeled with finite-rate chemical-kinetics, where the complexity of the kinetics model depends on the number of product species required from the analysis [Ajmani 2014b]. A realizable turbulence-model is used for turbulence closure [Shih 2008], and turbulence-chemistry interaction models are available for flows where said physics may need to be resolved [Liu 2013]. Ignition modeling is achieved with artificial ignition source terms introduced in a predetermined volume of the computational domain that is expected to contain a mixture of air and vaporized fuel.

CFD analysis with the NCC code was performed for the model N+3 combustor configuration and associated injector elements detailed in the previous section. All of the mesh-generation parameters and the NCC modeling parameters, including the finite-rate kinetics scheme, were identical to those reported for simulations conducted for an LDI based N+2 combustor [Ajmani 2014b]. This ensured that a useful comparison could be made between the emissions and performance of the model N+3 design and the previously analyzed N+2 design. This consistent approach also meet one of the goals of this work of leveraging the 'best practices' established in the extensive CFD analysis of previous LDI-1 and LDI-2 configurations with the NCC code.

3.1 Mesh Generation

- An all-tetrahedral mesh consisting of ~10M elements (~1M elements/injector) was generated with the CUBIT software (see figure 2). Best-practices of meshing optimization established in [Ajmani 2013a] were followed in the mesh-generation process.

3.2 Boundary Conditions

- Inflow: Fixed mass flow rate, static-temperature (T_3), turbulent kinetic energy and turbulent length scale
- Outflow: Fixed static pressure, (P_3-ΔP) (ΔP is set to 4% of the inlet pressure, P_3). All other flow quantities are extrapolated from the interior of the domain.
- Adiabatic, no-slip conditions at all solid walls

3.3 Liquid Fuel Modeling

- Each Simplex (Pilot, Main1) injector is modeled with SMD=8.8μm, V_{inj}=38.6m/s, 60° hollow cone with 10° cone thickness, 8 droplet groups, 32 streams/injector
- Each Airblast injector (Main2) is modeled as 16 'discrete' circumferential injection holes to model the annular fuel film, with SMD=7.5μm, V_{inj}=5m/s, 10° solid cone, 8 droplet groups, 8 streams/injector.
- The liquid spray was modeled by tracking spray particles in a Lagrangian framework, where each particle represents a group of actual spray droplets [Raju 2012]. The typical spray integration time-steps were 2e-7s (local time-step, *dtml*) and 4e-5s (global time-step, *dtgl*), which translates to 200 local time-steps for each global time-step for the spray solver.

3.4 Turbulence and Combustion Modeling

- Turbulence closure is obtained by using a two-equation, cubic k-ε model with variable Cμ [Shih 1998] and dynamic wall functions with pressure gradient effects [Shih 2000].
- The Jet-Fuel/Air mixture was lit by introducing ignition source-terms in a 1mm thick axial zone located 2mm downstream of the venturi exit of each of the nine injectors.
- A finite-rate kinetics mechanism calibrated for Jet-fuel combustion in LDI configurations [Ajmani 2014a] was used for direct, coupled computation of CO and NO. The chemistry model incorporates 14 species and 18 chemical reaction steps (see Appendix A). Jet-fuel was modeled as a surrogate mixture of decane (73%), benzene (18%) and hexane (9%).

4.0 CFD RESULTS FOR MODEL N+3 COMBUSTOR

CFD computations with the NCC are performed for two cycle-conditions corresponding to low-power and high-power operation of the model N+3 combustor. The first stage of each CFD simulation consists of non-reacting RANS computations with the boundary conditions and turbulence model detailed in section 3. The non-reacting RANS computations for the current N+3 setup (inlet mass flow rate = 0.0926kg/s, P_4 = 1.75MPa) converge at 60,000 steps, when run with CFL=1.95. Convergence is obtained when the mass-flow rate difference between outflow and inflow boundaries consistently remains below 0.1% over 500 consecutive iterations.

The effective area (AC_d) of the nine-element N+3 combustor, as computed by the predicted pressure drop (difference of inflow and outflow static pressure), the input mass-flow rate and the air density at the inflow, is computed from this converged solution. The predicted AC_d for non-reacting flow RANS CFD is 1.39in^2, which is <1% lower than the 'extrapolated' measured value of 1.4in^2. The 'extrapolated' AC_d is derived from measured LDI-2 data, after subtracting the individual effective area of the four injector elements that were deleted from the thirteen-element LDI-2 to obtain the model nine-element LDI-3 configuration studied here.

Reacting flow computations are initiated by using the converged non-reacting flow solution as an initial condition. The fuel spray is initiated for 100 iterations, at which point, the mixture is ignited by introduction of artificial ignition sources for 1000 iterations. An 18 step, 14 species finite- rate chemical kinetics (see Appendix A) is used for the reacting flow simulations. The reacting-flow RANS computations are run until the value of EINOx 'converges', as computed at the experimental 'measurement' plane of 114mm downstream of the dome. The EINOx is considered 'converged' when the variation in the mass-weighted average of NO mass-fraction at the 114mm plane is within a ±5% band for 1000 successive iterations. Convergence for the RANS simulations is obtained with an additional 150,000 reacting-flow steps beyond the initial 60,000 non-reacting steps, with a CFL=0.95.

4.1 CFD Results for 'Medium' Power Conditions

Emissions requirements for N+3 technology need to be evaluated for low-power, medium-power and high-power combustor operating conditions. Note that the low-power 'stages', i.e. the Pilot and Main stage, are identical for the current N+3 model combustor and the 'parent' N+2 combustor. Hence, performance and emissions at low-power (Idle) conditions for the N+3 combustor studied here will not differ from that of the N+2 combustor. The current CFD evaluation of the model N+3 combustor thus focuses on the performance and emissions at medium-power conditions. High-power emissions can be extrapolated from medium-power conditions, based on correlation equations reported by [Tacina 2014].

Axial-velocity and temperature contours from the RANS NCC predictions for *simulated* N+3 medium-power cycle conditions of P_3=1820kPa (264psi), T_3=950K (1250F) and FAR=0.0234 (ϕ=0.344), ΔP=4% are shown in figures 3 and 4. The axial-velocity contours show a strong central recirculation zones (CTRZ) behind the Pilot, and a weaker CTRZ behind the Main1 (M1) injectors. This behavior is attributed to the higher swirler angle of 55° for the Pilot element, as compared to 45° for the M1 injectors. In contrast, the axial velocity contours for the Main2 (M2) injectors show corner recirculation zones (CORZ) in the diverging section of the venturi for each airblast element with dual axial swirlers (45°CW/45°CW OAS/IAS).

These aerodynamics characteristics of the RANS CFD predicting strong CTRZ behind the simplex elements (and absence of CORZ) but strong CORZ behind the airblast elements (and absence of CTRZ), was also reported in previous LDI2 simulations of [Ajmani 2014b].

The temperature contours (figure 4) show that the Pilot and Main-1 stage with simplex injector (PA) elements have a relatively higher temperature, attached flames residing within (or near) the venturi. In contrast, the flames behind the Main-2 airblast (AB) injectors are relatively weaker. These differences in flame-anchoring behavior can be attributed to the presence of stronger CTRZ zones for the simplex elements (Pilot, Main1), and the lack of CTRZ for the airblast elements (Main2) (figs. 3 and 4). Similar differences in flame structures behind the simplex and airblast elements were also visualized during the experimental flame-tube testing of the LDI2 design at the Woodward FST facility.

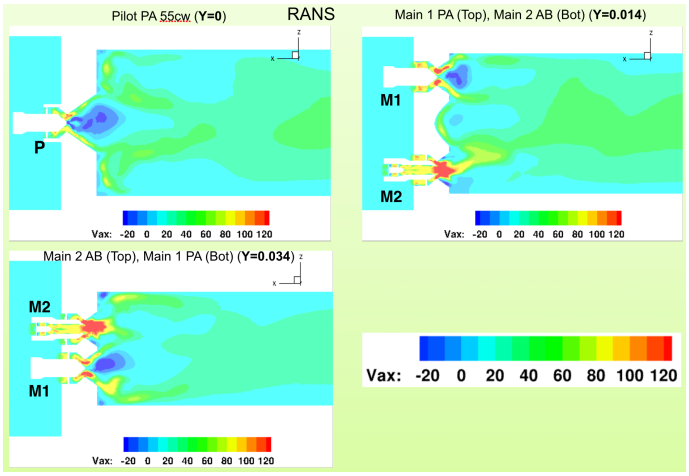

Figure 3. Axial velocity (m/s) contours for Pilot (P) and Main1 (M1)/Main2 (M2) axial cross-sections

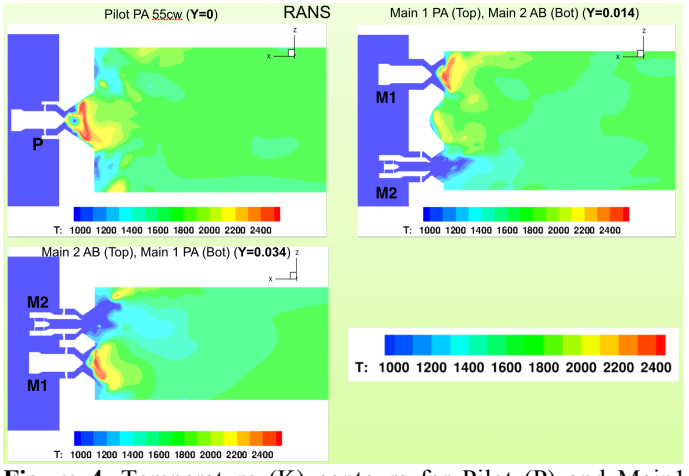

Figure 4. Temperature (K) contours for Pilot (P) and Main1 (M1)/Main2 (M2) axial cross-sections

NOx emissions of the model N+3 design, as indicated by NO mass-fraction contours along the length of the combustor at three axial slices, are shown in Figure 5. The Pilot injector seems to produce a large majority of the NOx, followed by the M1 stage. Both stages are fuel-fed by pressure-atomizing injectors. The M2 stage, fed by airblast injectors, produces the least amount of NOx. The NCC predictions indicate that most of the NOx produced in the vicinity of the venturis and the dome plate. The locations and relative intensities of NOx production behind the various injector elements can help guide optimization efforts in future iterations of the N+3 combustor design effort.

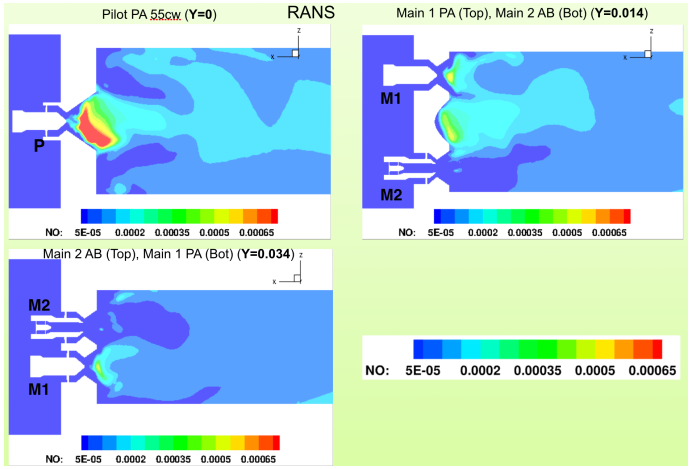

Figure 5. NO Mass-Fraction contours for Pilot and Main1 (M1)/Main2 (M2) axial cross-sections

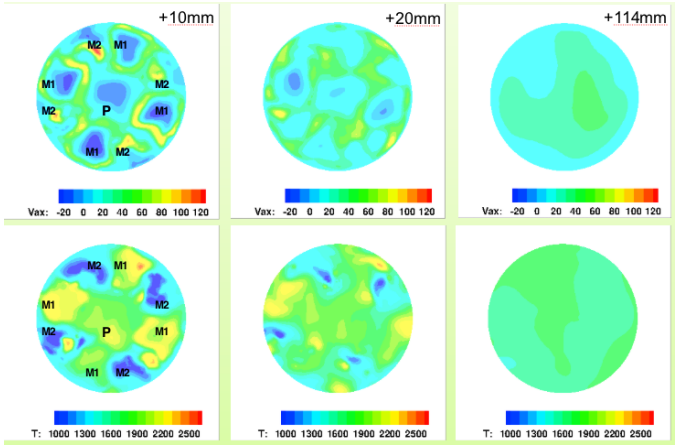

Figure 6. Axial velocity (min=-20, max=120m/s) (top) and Temperature (min=1000, max=2500K) contours (bottom) for three axial-locations downstream of the dump plane (+10mm, +20mm, and +114mm)

Figure 6 shows axial velocity (top) and temperature (bottom) contours at three axial locations downstream of the dump plane of the combustor. The strong central recirculation (CTRZ) behind the Pilot (P) and Main-1 (M1) injectors begins to diminish at the 20mm location, and the flow is fairly well

mixed by the 114mm location. Note that the 114mm plane was the reference location for collection of emissions data for the LDI2 flame-tube tests at NASA Glenn Research Center.

The temperature contours (Figure 6, bottom) show that the simplex-nozzle fueled Pilot (P) and Main1 (M1) stages dominate the heat release at the 10mm location. Further downstream, the temperature profile is fairly well mixed out at 114mm location. The NCC predicted combustor exit temperature (T_4) at the 114mm location is 1710K, which is within 1% of the *adiabatic* flame temperature of 1723K given by the CEA code [Sanford 1994] for the current simulated N+3 conditions (T_3=950K, FAR=0.0234).

Contours for NO and fuel ($C_{11}H_{21}$) mass-fraction are shown for axial locations of 10mm, 20mm and 114mm in figure 7. Most of the fuel is burnt by the 10mm location, and all the fuel is completely burnt at the 114mm location. The NO mass-fraction contours at 10mm indicate that the central Pilot (P) injector is responsible for the majority of the NO production for the combustor. As discussed earlier (see fig. 5), the four Main-1 elements produce much less NOx than the Pilot, and the four Main-2 elements produce negligible NOx.

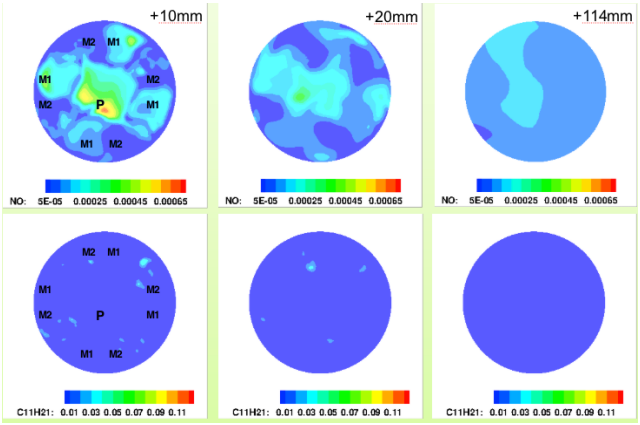

Figure 7. NO mass-fraction (min=5e-5, max=6.5e-4) (top) and Fuel mass-fraction (min=0.01, max=0.11) contours (bottom) for three axial-locations downstream of the dump plane (+10mm, +20mm, +114mm)

The predicted high NOx production of the Pilot element may be attributed to a combination of relatively long residence time and high temperature in the Pilot venturi. The longer axial length and stronger central recirculation zone (CTRZ) in the Pilot venturi contributes to the longer residence time. The choice of a shorter venturi length comparable to the venturi length of the Main elements, and a smaller swirler vane angle, could partly mitigate this behavior at high power conditions, at the probable expense of sacrificing the operability range of the Pilot at low-power conditions.

Experimental measurements at a comparable operating condition (T_3=810K, FAR=0.0261, ΔP=4%) for an N+2 combustor with the identical Pilot and Main1/Main2 stage injection elements used here, reported an EINOx (g of NOx per kg of fuel) value of 3.8 [Tacina 2014]. The NCC predicted value of EINOx is 6.6, when computed as a mass-weighted average of EINOx at the 114m plane, for the simulated medium-power condition (T_3=950K, FAR=0.0234, ΔP=4%).Type equation here.

In the absence of experimental data for the model N+3 combustor, the NCC predicted EINOx can be validated by a comparison with the EINOx prediction from the correlation equation derived by [Tacina 2014] for combustors operating with a combination of pressure-atomizing and airblast injectors. This correlation was derived from a large dataset of experimental flame-tube data obtained for the parent N+2 combustor used in this study, and is given below:

$$EINOx = p_3^{0.5}\, e^{T_3/230}\, (\Delta p/p)^{-0.6}\, (a_1\phi_1^{b1} + a_2\phi_2^{b2} + a_3\phi_3^{b3}) \quad (1)$$

a_1=0.0081, b_1=0.29, a_2=0.35, b_2=7.15, a_3=0.369, b_3=7.37

ϕ_1, ϕ_2, ϕ_3 are the equivalence ratios for the P, M1, M2/M3 stages.

For the N+3 model studied here, no M3 stage exists, so a_3=0.369/2

The N+2 correlation equation (1) predicts that the EINOx for the current nine-element N+3 configuration operating at T_3=950K, FAR=0.0234 (ϕ=0.3416, ϕ_1=ϕ_2=ϕ_3) would be 65% higher than that of the thirteen-element N+2 configuration operating at similar medium-power conditions of T_3=810K, FAR=0.0261 (ϕ=0.381, ϕ_1= ϕ_2=ϕ_3). Thus, the current NCC RANS prediction of 74% higher EINOx for the N+3 model combustor agrees reasonably well with 65% increase in EINOx suggested by the correlation equation from N+2 combustor experimental data.

5.0 COMPARISON OF NCC RANS AND TFNS/VLES

The steady-state RANS CFD analysis presented in previous sections of this paper was also compared with a Very Large Eddy Simulation (VLES) computation approach, using the Time-Filtered Navier-Stokes (TFNS) techniques available within the NCC code. The motivation for the computations reported in this section was to assess the differences in the non-reacting and reacting flow-fields, and emissions performance predictions of the model N+3 combustor, with NCC RANS and NCC TFNS.

The NCC TFNS approach is based on the concept of temporal filtering to enable a grid-independent very large eddy simulation ([Shih, 2009], [Liu, 2013]). In TFNS, the contents of both the resolved and unresolved turbulence are regulated by a "filtering control parameter" (FCP), which is related to the width of the temporal filter. At a given FCP (between 0.0 and 1.0), the resolved, very large scales of the turbulence are directly calculated, and the effects of the unresolved scales of the turbulence are modeled by a dynamic equation system. This approach leads to a unified simulation strategy for URANS, VLES, and LES by varying the value of the FCP in conjunction

with the use of a mesh that adequately supports the intended resolution based on the user-selected value of the FCP.

In practice, the choice of FCP in a TFNS solution depends on the flow-field ***and*** the available mesh resolution. If the chosen FCP is too small, the solver may give erroneous results as the method attempts to resolve length scales that are smaller than the smallest mesh-size. If the chosen FCP is too large, the solver may not resolve enough of the turbulent length scales of interest and reverts to an unsteady RANS solution. For a linear turbulence model, the physical effect of FCP can be represented in the *modeled* turbulent viscosity (μ_t) as

$$\mu_t = f(\text{FCP}) * (C_\mu \rho k^2 / \varepsilon)$$
$$\text{where } f(\text{FCP}) = 2*\text{FCP} - \text{FCP}*\text{FCP}$$

C_μ is a modeling constant (typically set to 0.09), and ρ, k and ε are the density, turbulent kinetic energy and turbulent dissipation-rate of the flow, respectively.

A converged non-reacting RANS solution (see previous section) is used as a starting point for the TFNS computations. An unsteady RANS (URANS) solution with a fixed time-step of 1.0μs for 10000 time-steps is computed. This URANS solution is then used to initiate the TFNS solution with the NCC. Based on the detailed study reported in [Ajmani 2013b] of the effect of FCP on solution accuracy for LDI flows, a value of FCP=0.30 is used for the TFNS solutions presented here.

Figures 8 and 9 show axial-velocity velocity contours for the NCC TFNS solution, as an average of the final 20000 time-steps of a 45000 time-step solution (Δt=1e-6s). Note that, in contrast to the RANS solutions, the TFNS predicts the expected flow symmetry about the centerlines for the Pilot, Main1 and Main2 elements. The TFNS also predicts fairly identical recirculation zones (CTRZ) behind all the M1 and M2 elements, as compared to large variations predicted by RANS.

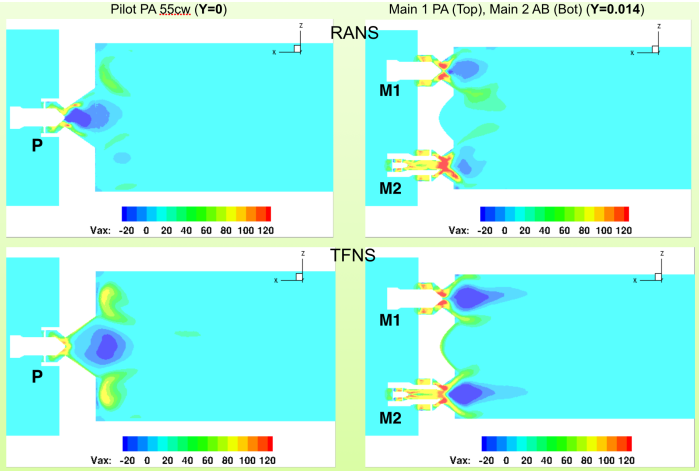

Figure 8. Axial velocity (m/s) contours for RANS (top) vs. TFNS (bottom): Pilot (P) at y=0 (left) and Main1 (M1)/Main2 (M2) swirlers at y=0.014m (right) axial sections

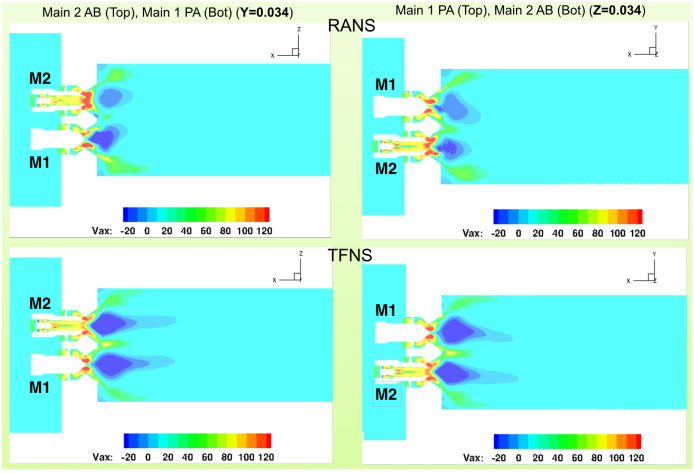

Figure 9. Axial velocity (m/s) contours for RANS (top) vs. TFNS (bottom): Main1 (M1)/Main2 (M2) swirlers at y=0.034m (left) and z=0.034m (right) axial sections

Comparisons of the predicted non-reacting flow velocity profiles at various axial locations downstream of the combustor dump plane for RANS NCC and TFNS are shown in figures 10. At the 10mm and 20mm locations, the CTRZ behind all nine injectors is much stronger for the TFNS, as compared to the RANS predictions. The TFNS solution predicts very well defined flow structures (10mm location) behind each of the nine elements. The RANS solution predicts much faster inter-element mixing as compared to the TFNS, as seen at the 20mm location. Both the RANS and TFNS solutions predict a well-mixed flow velocity profile at the experimental measurement plane (114mm).

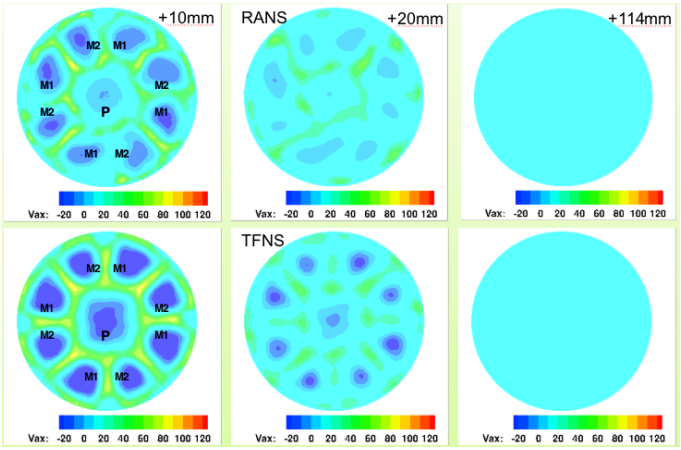

Figure 10. Axial velocity (m/s) contours for RANS (top) and TFNS (bottom): l0mm, 20mm, 30mm downstream of dome

In summary, the comparison of NCC RANS and TFNS for *non-reacting* flow shows that the TFNS predicts more consistent flow structures for the N+3 model combustor. However, the higher fidelity of TFNS comes at the cost of computational resources. The computational cost of *non-reacting* TFNS is 2x to 3x more than that of a comparable

RANS computation. Preliminary *reacting-flow* computations of the N+3 model combustor with NCC TFNS indicated a 10x increase in computational time over that of a reacting-flow NCC RANS solution.

This added computational time for NCC TFNS can quickly become prohibitive when performing full-scale CFD analyses of multiple parametrics during the preliminary design stages of a new combustor. Hence, the use of *reacting-flow* TFNS may be best suited to the latter stages of N+3 combustor design analysis, or optimization of individual combustor components e.g. a single-injector of a multiple-injector configuration. This strategy of using RANS for parametric analysis can save considerable CFD resources, and is partly justified by the reasonable emissions predictions provided by NCC RANS for the model N+3 combustor studied here (see section 4.1).

6.0 SUMMARY AND RECOMMENDATIONS

An initial CFD evaluation of a model combustor to meet NASA's emissions, operability and durability goals for small core size and high pressure-ratio (>50) N+3 combustors was conducted in this study. Lessons learned from previous generation (N+1, N+2) design efforts leveraging Lean Direct Injection (LDI) technology were adapted for the N+3 model LDI combustor proposed in this work. Emissions predictions for a typical 'medium' power N+3 cycle condition, which has a nominal 17% higher inlet temperature (T_3) as compared to an N+2 cycle, indicate a 74% increase in EINOx for the model, *non-optimized* N+3 combustor over a 'parent' N+2 combustor *optimized* for NOx emissions.

The CFD analysis predicts that a majority of the EINOx was produced by the central pilot injection element, with the neighboring array of Main injection elements producing relatively negligible EINOx. Future efforts at emissions reductions for the model N+3 combustor could focus on optimizing the geometry and/or choice of fuel-injector strategy for the Pilot element. This optimization could be done by replacing the pressure-atomizing pilot with an airblast injector, reducing the blade-angle of the pilot, recessing the pilot and/or the Main1/Main2 stage(s) from the combustor dome, or a combination of these approaches. In addition, future work could evaluate the effect of varying the inter-element spacing (the packing factor at the combustor dome) on the performance and emissions of the model N+3 combustor studied here.

From a CFD modeling perspective, efforts are being targeted at reducing the computational cost of the higher-fidelity and higher-accuracy TFNS approach of the NCC, in order to make it feasible as a default go-to approach to for LDI combustor simulations. The implementation of compact chemical kinetics schemes and liquid spray models for alternate fuels forms an integral part of ongoing efforts with the NCC. The goal is to enable timely, relevant CFD inputs that will reduce the design costs of next-generation N+3 combustors.

7.0 ACKNOWLEDGEMENTS

This work was funded by NASA Glenn Research Center's Subsonic Fixed Wing project, and all computations were performed at NASA's NAS Supercomputing Facility.

8.0 REFERENCES

[Ajmani 2013a] Ajmani, K., Mongia, H.C. and Lee, P., "CFD Best Practices to Predict NOx, CO and Lean Blowout for Combustor Design," ASME IGTI Paper GT2013-95669, ASME Turbo Expo 2013, San Antonio TX, June 2013.

[Ajmani 2013b] Ajmani, K., Mongia, H.C. and Lee, P., "Evaluation of a Very Large Eddy Simulation (VLES) CFD Approach for LDI Combustor Analysis," AIAA Paper 2013-3688, 49th AIAA Joint Propulsion Conference & Exhibit, San Jose CA, July 2013.

[Ajmani, 2014a] Ajmani, K., Mongia, H. C., and Lee, P., "CFD computations of emissions for LDI-2 combustors with simplex and airblast injectors", AIAA Paper 2014-3529, 50th AIAA Joint Propulsion Conference, July 2014.

[Ajmani 2014b] Ajmani, K., Kundu, K., and Yungster, S., "Evaluation of Reduced Mechanisms for Combustion of Jet-A in LDI Combustor CFD Calculations," AIAA Paper 2014-3662, AIAA Propulsion and Energy Conference, Cleveland, OH, July 2014.

[Lee 2007] Lee, C. -M., Tacina, K.M. and Wey, C., "High Pressure Low NOx Emissions Research: Recent Progress at NASA Glenn Research Center," ISABE 2007-1270.

[Lee 2013] Lee, C. -M., Chang, C., Kramer, S., and Hebron, J.T., "NASA Project develops next generation low-emission Combustor Technologies," 51st AIAA Aerospace Sciences Meeting, Dallas TX, AIAA Paper 2013-0540.

[Liu 2011] Liu, N. -S., Shih, T. -H., and Wey, C.T., "Numerical Simulations of Two-Phase Reacting Flow in a Single- Element Lean Direct Injection (LDI) Combustor Using NCC", NASA/TM 2011-217031, NASA Glenn Research Center.

[Liu 2013] Liu, N. -S., Wey, C.T., and Shih, T. -H., "Time-Filtered Navier-Stokes Approach and Emulation of Turbulence-Chemistry Interaction," 51st AIAA Aerospace Sciences Meeting, Dallas TX, AIAA Paper 2013-0707.

[Liu 2014] Liu, N. -S and Wey, C.T., "On the TFNS Subgrid Models for Liquid-Fueled Turbulent Combustion", AIAA Paper 2014-3569, AIAA Propulsion and Energy Conference, Cleveland, OH, July 2014.

[Sanford, 1994] Sanford, G., and McBride, B., "Computer program for calculation of complex chemical equilibrium

compositions and applications. Part 1: Analysis", NASA-RP-1311, 1994.

[Shih 1998] Shih, T. -H., Chen, K. -H., Liu, N. -S., Lumley, J. L., "Modeling of Turbulent Swirling Flows," NASA-TM 1998–113112.

[Shih 2000] Shih, T.-H., Povinelli, L.A., Liu, N.-S and Chen, K.-H., "Generalized Wall Function for Complex Turbulent Flows," NASA TM 2000-209936.

[Shih 2009] Shih, T. -H. and Liu, N. -S., "A Nonlinear Dynamic Subscale Model for PRNS/VLES of Internal Combustor Flows," AIAA–2009–0467, January 2009, Orlando, FL.

[Tacina 2005] Tacina, R., Lee, P., and Wey, C., "A Lean-Direct-Injection Combustor Using a 9 Point Swirl-Venturi Fuel Injector," ISABE 2005-1106.

[Tacina 2014] Tacina, K.M., Chang, C., He, Z.J., Mongia, H.C., Dam, B., and Lee, P., "A Second Generation Swirl-Venturi Lean Direct Injection Combustion Concept," AIAA Paper 2014-3434, AIAA Propulsion and Energy Conference, Cleveland, OH, July 2014.

[Zink 2014] Zink, G.A., Ryon, J.A., and Pack, S.D., "Intermediate Pressure Combustion Research of a Multipoint Low NOx Combustion System," AIAA Paper 2014-3629, AIAA Propulsion and Energy Conference, Cleveland, OH, July 2014.

APPENDIX A

A finite-rate chemistry model was used to compute the species source-terms for Jet-A/air chemistry [Ajmani 2014b]. Reacting flow computations were performed with the chemical-kinetics model described in Table 1. The chemistry model incorporates 14 species and 18 chemical reaction steps. Jet-A fuel is modeled as a surrogate mixture of decane (73%), benzene (18%) and hexane (9%).

The kinetics model uses **A** (pre-exponential factor), **n** (temperature exponent) and **E** (activation energy, cal/mol) to compute the Arrhenius rate coefficient, $\mathbf{k = A\ (T/T_0)^n\ e^{(-E/RT)}}$, for a given temperature, **T** (K). (**R** = universal gas constant, $\mathbf{T_0}$ (K) is a reference temperature). Note that reaction steps 1-3 are irreversible, and reaction steps 4-18 are formulated as reversible reactions. The kinetics for NOx prediction includes an extended Zeldovich mechanism (four steps for NO) and an additional four steps for N_2O species. The inclusion of N_2O is expected to improve the NOx predictions in the small local regions where fuel-rich burning is occurring in the flow.

	Reaction	A	n	E
1	C11H21 + O2 => 11CH + 10H +	1.00E+12	0.00	3.10E+04
	GLO / C11H21 0.8/			
	GLO / O2 0.8/			
2	CH + O2 => CO + OH	2.00E+15	0.00	3.00E+03
3	CH + O => CO + H	3.00E+12	1.00	0.00E+00
4	H2 + O2 <=> H2O + O	3.98E+11	1.00	4.80E+04
5	H2 + O <=> H + OH	3.00E+14	0.00	6.00E+03
6	H + O2 <=> O + OH	4.00E+14	0.00	1.80E+04
7	H2O + O2 <=> 2O + H2O	3.17E+12	2.00	1.12E+05
8	CO + OH <=> CO2 + H	5.51E+07	1.27	-7.58E+02
9	CO + H2O <=> CO2 + H2	5.50E+04	1.28	-1.00E+03
10	CO + H2 + O2 <=> CO2 + H2O	1.60E+14	1.60	1.80E+04
11	N + NO <=> N2 + O	3.00E+12	0.30	0.00E+00
12	N + O2 <=> NO + O	6.40E+09	1.00	3.17E+03
13	N + OH <=> NO + H	6.30E+11	0.50	0.00E+00
14	N + N + M <=> N2 + M	2.80E+17	-0.75	0.00E+00
15	H + N2O <=> N2 + OH	3.50E+14	0.00	7.55E+02
16	N2 + O2 + O <=> N2O + O2	1.00E+15	0.00	3.02E+02
17	N2O + O <=> 2NO	1.50E+15	0.00	3.90E+04
18	N2O + M <=> N2 + O + M	1.16E+15	0.00	3.32E+04

Table 1: Kinetics mechanism for Jet-A fuel surrogate used for NCC emissions computations